

THE CALCULATION OF THE NEUTRON TRANSMISSION THROUGH THE ACCESS WAY OF A HIGH-ENERGY ACCELERATOR INSTALLATION (USING THE MORSE CODE)

YE SIZONG*

CERN, 1211 Geneva 23, Switzerland

(Received November 30, 1981; in final form February 18, 1982)

The MORSE code (Multigroup Oak Ridge Stochastic Experiment) was used to calculate the attenuation of radiation in an access tunnel of a high-energy proton accelerator (NIMROD). A monoenergetic isotropic neutron point source was used to simulate the radiation source produced by the interaction of high-energy protons with a copper target. Different source energies (1.5 MeV, 10 MeV, 20 MeV) were chosen for the calculation. The results of these calculations agree well with measurements and with a "universal attenuation curve" for the second leg of the tunnel. It seems that the MORSE code can be used to simulate the transport of neutrons in the second leg and onwards in a tunnel of a high-energy accelerator installation, independently of the source energy (when the source energy is above 4 MeV).

From the calculated spectra it can be seen that a quasi-equilibrium neutron spectrum appears from about 2.5 m onwards in the second leg, and up to 45% of the total dose equivalent in the second leg comes from the neutrons with energies ranging from 0.15 MeV to 2 MeV.

1. INTRODUCTION

In a high-energy accelerator installation there must always be ducts for cables, ventilation, etc., and access ways for personnel and components through the main shield of the accelerator. These ducts and access tunnels can also act as leakage paths for radiation, especially low-energy secondary neutrons; therefore, the design of ducts and access ways has to match the requirements of radiation protection as well as those of the accelerator functions.

There have been many excellent measurements of radiation attenuation in access tunnels of high-energy accelerators.¹⁻⁴ There are also many computer codes which can estimate the attenuation of neutrons in access tunnels and ducts, e.g., AMC,⁵ SAM-CE,⁶ ZEUS,⁷ MORSE,^{8,9} etc. In this paper the MORSE code was used to calculate the neutron transport in a concrete-lined tunnel of the experiment of Stevenson and Squier.¹ An isotropic neutron point source was used to simulate the radiation source produced by the interaction of high-energy protons with the copper target. The geometry and the source will be described in detail in Sections

2 and 3. A brief introduction to the MORSE code and its application to the calculation of access tunnel radiation attenuation is given in Section 4. In Section 5, all the results are listed or illustrated.

2. THE DESCRIPTION OF THE SOURCE AND THE GEOMETRY

The experiment of Stevenson and Squier¹ at the Rutherford Laboratory was chosen for comparison because this measurement was done in a tunnel with a single right-angled bend, with clean source geometry, and using many well-calibrated activation detectors [$^{12}\text{C}(n, 2n)^{11}\text{C}$, $^{19}\text{F}(n, 2n)^{18}\text{F}$, $^{27}\text{Al}(n, \alpha)^{24}\text{Na}$, $^{197}\text{Au}(n, \gamma)^{198}\text{Au}$, indium activation in a wax moderator, etc.]. The description of the geometry of the tunnel given in the original article¹ is repeated here.

This experiment was done in the X3 extracted proton beam line of the 7 GeV synchrotron NIMROD, in which a well-defined source was used to determine the attenuation in a large tunnel of moderate length. The tunnel was constructed as part of the normal extracted beam blockhouse at right angles to the direction of the beam as shown in Figs.

* Permanent address: Institute of High-Energy Physics, Academia Sinica, Beijing, People's Republic of China.

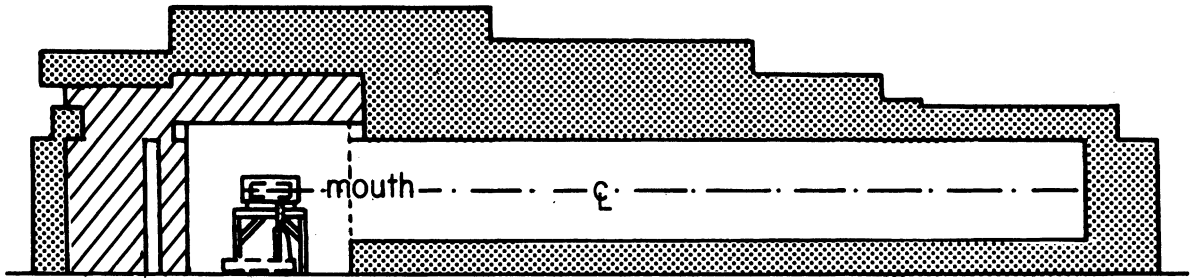


FIGURE 1 Vertical section of the NIMROD tunnel.

1 and 2.* The tunnel contained a right-angled bend at 11 m from the mouth, with a second leg 8 m long. The tunnel cross section was $2.3 \times 2.3 \text{ m}^2$. The inner surface consisted of concrete (density $\sim 2.3 \text{ g/cm}^3$). The extracted beam target was situated on the center line of the tunnel 1.9 m from its mouth. The tunnel roof was approximately 40 cm lower than the blockhouse ceiling, and the

tunnel floor 75 cm higher than normal floor level.

3. THE SIMPLIFICATION OF GEOMETRY AND SOURCE

3.1 *The Source*

The albedo of the high-energy neutrons (with energy greater than 20 MeV) is small; the other kinds of charged particles emitted from the target

* Also Figs. 1 and 2 of this paper.

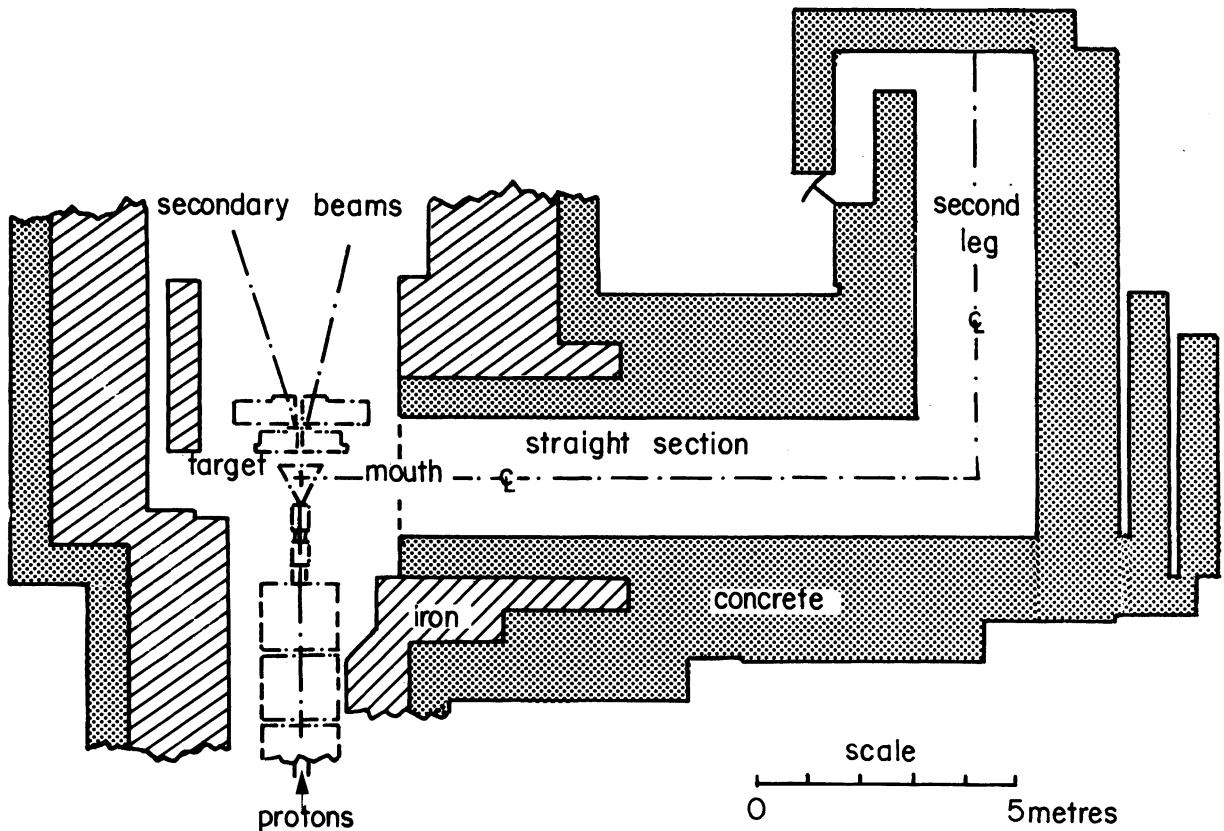


FIGURE 2 Plan view of the NIMROD tunnel.

also possess this character. Furthermore, the energy of the particles "scattered back" from the wall is much lower than that of the incident particles. From this it can be deduced that from the second leg onwards, fast neutrons (i.e., neutrons of less than 20 MeV) would dominate the dose equivalent. Some experiments also proved this deduction. For example, the data of Ref. 1 show that at a depth of 1.7 m from the mouth in the second leg, the ratio of the flux detected by ^{11}C (neutrons with $E > 20$ MeV) to the flux detected by moderated indium (activation of indium foils in a wax moderation which thus detects neutrons with energies below several MeV) was about 1%, and the ratio of the dose rates about 5%. At the mouth of the second leg, the ratio of these two fluxes is 12.5% and the ratio of the doses is about 60%. In the experiment, the target was located just opposite and 1.9 m away from the mouth of the access tunnel. This target may be thought of as a point source. The neutrons of several MeV energy result from evaporation neutrons which are emitted isotropically. It therefore seems to be a good approximation that an isotropic fast-

neutron point source was used instead of the real target.

3.2 The Geometry

The principal simplifications concerned the structure of the main ejected beam tunnel. As shown in Fig. 3, this tunnel was assumed to be of uniform rectangular cross section, 4 m wide and 3.45 m high, surrounded by concrete walls.

In order to reduce the computing time, another simplification was made, namely that all the walls were taken to be 0.6 m thick. According to Vogt,¹⁰ the albedo of fast neutrons on a concrete slab of 0.6 m thickness is almost the same as on one of 1 m thickness (effectively a semi-infinite wall). The difference in the energy spectra of back-scattered neutrons appears only at the low-energy end (below 50 eV). As will be seen below, this difference does not significantly affect the total dose equivalent.

4. MONTE CARLO CODE MORSE

4.1 Code Description

MORSE (the Multigroup Oak Ridge Stochastic Experiment code)^{8,9} is a multipurpose neutron and gamma-ray Monte Carlo code. It was written in FORTRAN IV and has versions for the IBM 370 and the CDC 6600 (only the IBM 370 version is operative at CERN).

By the use of multigroup cross sections, all the interaction processes (including the generation of secondary gamma) become transfers from one energy group to another. The gamma rays may be considered as particles in the energy groups with group numbers greater than the maximum group number for neutrons. For anisotropic scattering, each group-to-group transfer has an associated angular distribution which is a weighted average over various cross-sections involved in the energy transfer process. Thus the multigroup cross sections have the same format for both neutrons and gamma rays, and the random walk process (the process used to transport neutrons or gamma photons from one collision to another) possesses the same logic. The possible transport cases that can be treated are neutrons only, gamma rays only, coupled neutron-gamma rays, gamma rays from a coupled set and fission, for either a forward or adjoint case and for isotropic or anisotropic scattering up to a P_{16} Legendre expansion of the angular distribution.

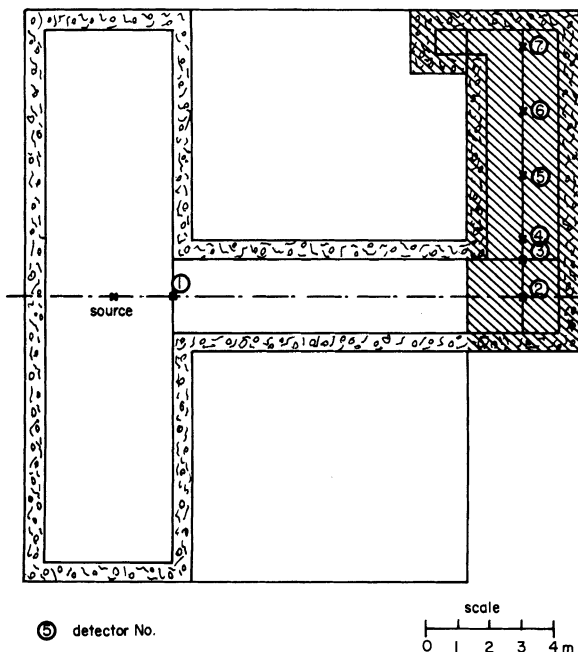


FIGURE 3 The geometry used in the calculations. All the detectors are on the center line of the tunnel and on the same level as the source, with 1) at the mouth of the first leg; 2) 11 m from the mouth of the first leg; 3) at the mouth of the second leg; and 4), 5), 6), and 7) 0.7 m, 2.7 m, 4.7 m, and 6.7 m from the mouth of the second leg, respectively.

In the MORSE code there is already an albedo module which, when used, does a specular reflection at the entry of a particle into a specified medium.

Several types of importance-sampling techniques are included in the code. They are

- i) Russian roulette and splitting. These can be implemented together or separately in specified regions or energy groups.
- ii) Exponential transform. The parameters, the energy group, and the regions can be chosen by the user.
- iii) Source energy biasing and energy biasing at each collision are also options.

As a result, the code calculates the spectrum—neutrons or gamma photons per eV in various energy groups. Then, according to the response functions given by the user, and using the determined spectrum, the code calculates the corresponding responses for different kinds of detectors (e.g., count, absorbed dose, dose equivalent, the responses of various activation detectors). If desired, an angle- and energy-dependent fluence can also be obtained.

4.2 Application to Duct Calculation

Because the ready-made albedo module in the code can offer only a specular reflection at the boundary between two media (which is too far from the real physical process), the albedo technique was not used in these calculations even though it may be the best for duct calculation. Importance-sampling was kept to a minimum because the author wanted to keep the physical model used in the calculation as close to the real one as possible in order that the result obtained from the calculation could be comparable with the measurement. Because of the large computer-time consumption of this code, it was almost impossible to trace the entire neutron history. Therefore, some unimportant neutrons, e.g., thermal neutrons, had to be ignored, and some moderate importance-sampling techniques were used so that the calculation could be managed in an acceptable computer time.

4.2.1 The Reduction of Wall Thickness Neutrons which penetrate deeply into the wall, even if they could be scattered back out of the wall (the probability is very small), would not give any significant contribution to the dose at

the points of interest in the access tunnel. From the point of view of radiation protection they can be ignored. Thus all the walls surrounding the tunnel were taken as 0.6 m thick in this calculation.¹⁰

The code was slightly modified in order to make the "external void" act as an "absolute neutron absorber." Once a neutron enters into this imaginary medium, i.e., outside the regions of interest, it is assumed to be absorbed. Consequently the history of the neutron is finished. Also, if there is such an "external void" between a collision point and a detector position, the contribution in the next event estimator is thought of as zero (i.e., it is impossible for neutrons to penetrate through it, no matter how thick it is).

As the walls of the NIMROD tunnel were rather thick (2–3 m), the probability of neutrons penetrating into the second leg is several orders of magnitude lower than the probability of their being scattered from the inner surfaces of the walls. Thus this simplification was reasonable.

4.2.2 Direction Biasing of Source Neutrons

The source was assumed as isotropic for this calculation; however, source neutrons emitted in different directions are not all of the same importance. Considering especially the dose in the second leg, only those neutrons which travel towards the tunnel mouth can give a significant contribution. Thus a source direction biasing could be applied here.

For this purpose a cone with the source point as the vertex was drawn (see Fig. 4). Let us assume that the contribution of the source neutrons with direction cosines outside the cone could be

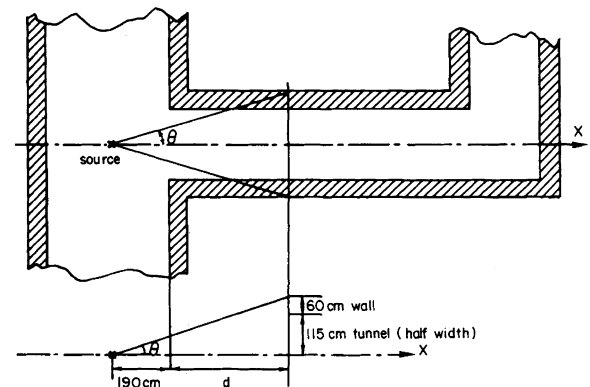


FIGURE 4 The geometry used in testing the source direction biasing.

neglected. (In the program, only those source neutrons inside the cone were accepted and followed, whilst the others were rejected.) Obviously, an additional weight $\Omega/4\pi$ should be put on these accepted source neutrons; here Ω is the solid angle contained by the cone and

$$\Omega = 2\pi(1 - \cos \theta). \quad (1)$$

Here θ is the semi-vertex angle of the cone (see Fig. 4).

Several tests with different semi-vertex angles θ were carried out. The results are listed in Table I. A quantity Q is usually used as an efficiency index for different biasing techniques

$$Q = T \cdot \sigma^2,$$

where T is the consumed computer time for the run;

σ is the relative standard deviation of a certain physical quantity obtained from the run.

From Table I it can be seen that as the value of $\cos \theta$ increased from 0.70 to 0.88, there appeared to be a drastic increase of the efficiency. But in the case of $\cos \theta = 0.96$, the biasing was so severe that the result (fluence, dose, etc.) was underestimated. Finally, in the calculation, a source direction biasing with $\cos \theta = 0.92$ was adopted to calculate the responses of detectors deep in the second leg. In the first leg, especially near the mouth, the source neutrons travelling in a direction outside the cone cannot be neg-

lected. Therefore, no source direction biasing was used in the calculations for the first leg.

4.2.3 Russian Roulette and Splitting As the neutron energy decreases, the neutron fluence per unit of dose equivalent increases rather quickly. For example, the conversion factor for a 10 MeV neutron is $6.8 \text{ n}\cdot\text{cm}^{-2} \text{ s}^{-1}/\text{mrem}\cdot\text{h}^{-1}$ (or $4.08 \times 10^{-8} \text{ rem}/\text{n}\cdot\text{cm}^{-2}$), and for a 10 keV neutron $283 \text{ n}\cdot\text{cm}^{-2}\cdot\text{s}^{-1}/\text{mrem}\cdot\text{h}^{-1}$ (or $9.82 \times 10^{-10} \text{ rem}/\text{n}\cdot\text{cm}^{-2}$). The latter is only 2.4% of the former. From this it can be foreseen that the lower-energy neutrons are less important for the dose equivalent. (This quantity is the most interesting one for radiation protection.) There is therefore no need to calculate these lower-energy neutrons in detail. In this calculation, when the neutrons were down-scattered to the energy group number 28 (0.01 MeV) or below, Russian roulette was played. The parameters of Russian roulette were chosen so that the surviving probability was about 1/5. From the result (see Section 5), we can see that the contribution of neutrons with energy group numbers 28 to 36 was about 5% to 10% of the total dose equivalent.

4.2.4 The Cross Section The multigroup cross section data file used in this calculation is DLC-31/FEWGI¹¹ obtained from the Data Library Collection of RSIC (the Radiation Shielding Information Center). These data were tested against typical transport problems in air and concrete.¹²

The compositions of concrete and air used for this calculation are listed in Table II.¹³

TABLE I
The Efficiency of Source Direction Biasing

cos θ		0.70	0.88	0.92	0.96
θ		45°34'23"	28°21'27"	23°4'26"	16°15'37"
$d(\text{cm})^a$		-18.5	134	221	410
W_{start}		0.15	0.06	0.04	0.02
Source samples		18,000	12,800	3,000	6,000
Computer time (s/200 n)		14	25.5	25	16
Detector No. 6	Count	2.39×10^{-9}	2.82×10^{-9}	2.65×10^{-9}	2.07×10^{-9}
	Moderated In	3.59×10^{-9}	3.89×10^{-9}	3.57×10^{-9}	2.91×10^{-9}
	rem	3.67×10^{-17}	3.62×10^{-17}	3.36×10^{-17}	3.08×10^{-17}
	$T \times \sigma^{2b}$	85.2	5.88	4.54	5.81
		35%	6%	11%	11%
		26%	6%	11%	11%
		8%	6%	10%	11%

^a d is the distance from the mouth of the first leg to the base of the cone, see Fig. 4.

^b σ is the relative standard deviation for the response of moderated indium.

Note. All the results were normalized to one source neutron. The percentage is the relative standard deviation. The unit for count is: $\text{n}\cdot\text{cm}^{-2}$ per source neutron; for moderated In: counts per source neutron; for rem: rem per source neutron.

TABLE II
Composition of Concrete and Air¹³
(unit: atoms/cm³)
($\times 10^{-24}$)

Element	Content	
	Concrete ($\rho = 2.43 \text{ g/cm}^3$)	Air ($\rho = 0.00129 \text{ g/cm}^3$)
Si	2.015×10^{-2}	
O	4.587×10^{-2}	1.128×10^{-5}
Al	1.743×10^{-3}	
H	9.30×10^{-3}	
Ca	2.660×10^{-3}	
N		4.195×10^{-5}

4.2.5 The Point Detector Estimator Because of the high efficiency of the point detector estimator (or next event estimation) (see, for example, Ref. 9), it was used for scoring in this calculation. Because all the detectors were situated along the centre line of the tunnel, 1.15 m from the wall and in air, this scoring method could give quite good mathematical results.

5. RESULTS

The results of calculations are illustrated in Figs. 5 to 17.

Because of the element cross-section data available from the DLC-31/FEWGI Library file, the random walk logic used in the MORSE code, and the group-to-group transport, the program cannot treat the thermal neutrons in detail. It does not allow upscattering in energy (except in an adjoint problem), but it has the option to trace the neutrons in the thermal energy group (group number 37) without energy degradation (i.e., just in the same energy group) until they are either absorbed, or retire, or escape from the system. To trace the thermal neutrons (even in the way described above) needs an unacceptable amount of computer time. Also, from the point of view of radiation protection the thermal neutrons are not the critical component in the duct calculation (subject to the fact that the most ordinary shielding material—concrete—is used as the extra

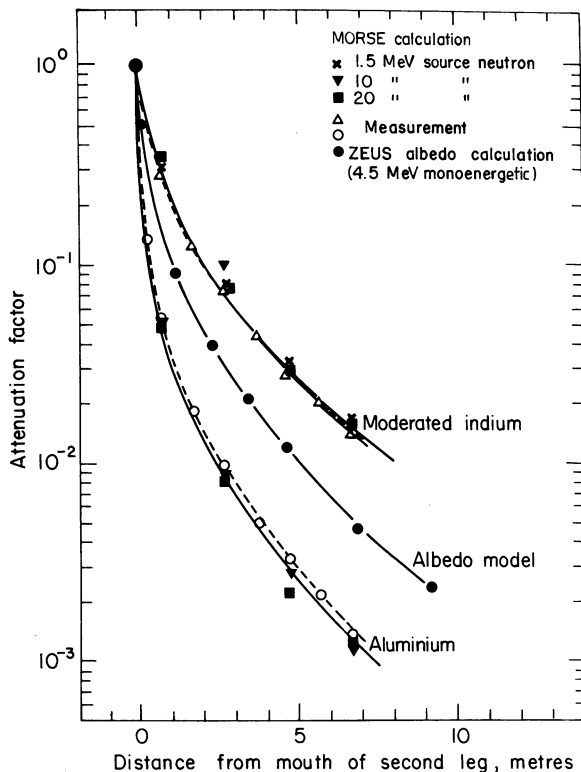


FIGURE 5 The calculated neutron attenuation in the second leg compared with the measurements. All data normalized to unity at zero distance.

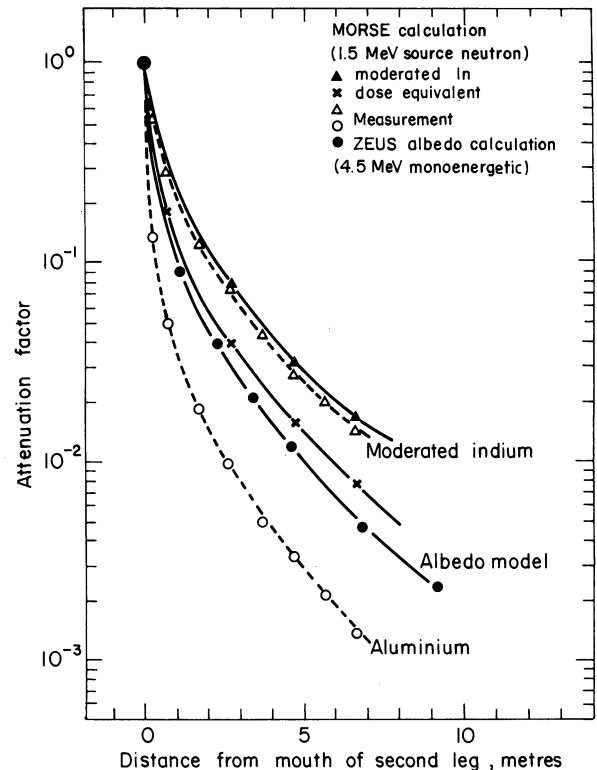


FIGURE 6 The normalized result of the calculations compared with the measurements in the second leg, with a source neutron energy $E_0 = 1.5 \text{ MeV}$.

shield, e.g., the lid on the entrance of an access tunnel). Thus this calculation did not go down to the thermal energy (this means the neutrons with energy below 0.414 eV in the DLC-31/FEWGI cross-section library file). But an "exploratory" test was done for the 10 MeV source neutrons in order to get some idea of the contribution of thermal neutrons to the dose equivalent. The result showed that the thermal neutrons contributed about 5% to the total dose equivalent and about half to the total flux at the point of detector number 7 (6.7 m deep in the second leg, see Fig. 3). This seems to coincide with Vogt's work,¹⁰ in which it was shown that the thermal neutrons contributed 3-4% to the total dose and about half to the flux at a moderate depth within the second leg for 15 MeV source neutrons.

Figures 5 to 9 show the results of calculation for 1.5 MeV, 10 MeV, and 20 MeV source neutrons compared with the measurement in the second leg of the tunnel. The points displayed as "calculation" have been obtained by folding the response curves of the different "detectors" with the calculated differential flux density; they are

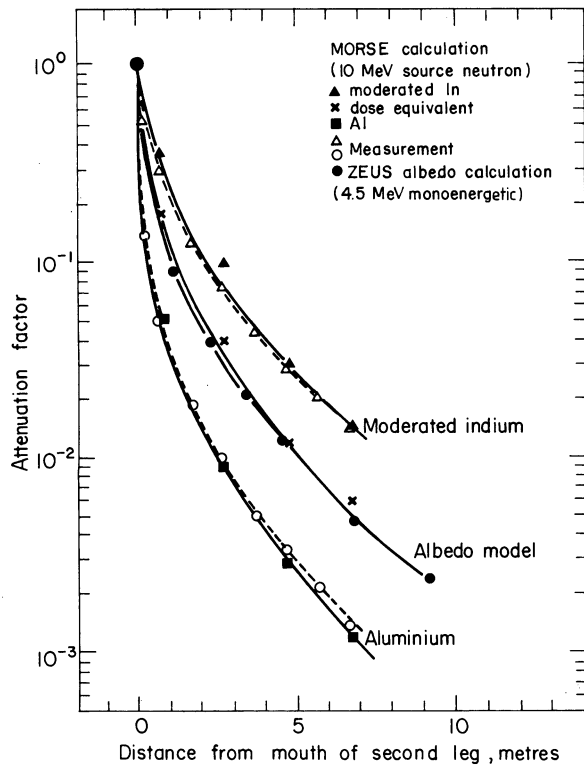


FIGURE 7 Same as Fig. 6, with $E_0 = 10$ MeV.

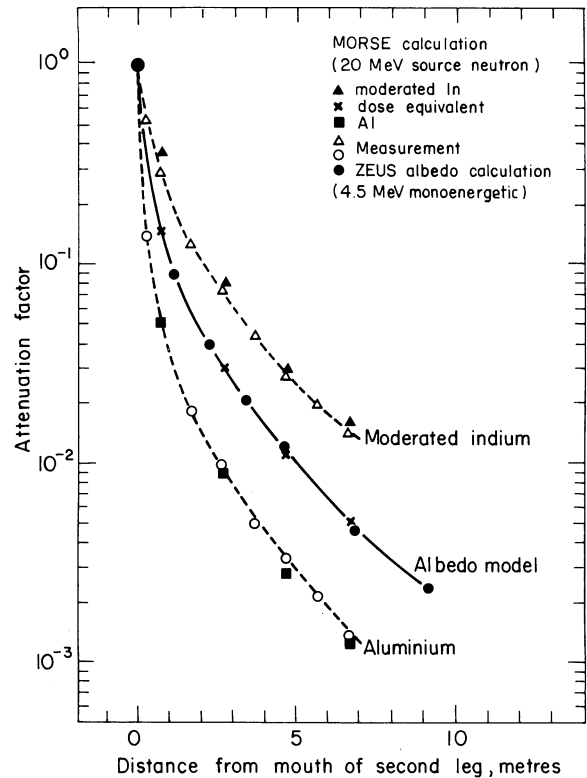


FIGURE 8 Same as Fig. 6, with $E_0 = 20$ MeV.

normalized to unity at zero distance (mouth). For moderated indium the response curve reported by Hargreaves and Stevenson,¹⁴ for aluminium the evaluated cross-section curve of BNL 325,¹⁵ and for dose equivalent the curve recommended by ICRP¹⁶ were used. The points marked "measurements" refer to measurements of Stevenson and Squier¹ of the induced specific activity in the detectors, corrected for decay and saturation and normalized to unity for zero distance in legs. The predictions of dose equivalent attenuation made by Gollon and Awschalom,¹⁷ using the ZEUS albedo programme with a single energy group (4.5 MeV), are also presented.

In Fig. 9 additional experimental attenuation data reported in Ref. 1 are presented. Instead of the moderated In and dose-equivalent attenuation measurements, activation data in carbon, fluorine, and gold are displayed, showing the attenuation for different reaction thresholds in the first and second legs. In this figure the MORSE-calculated points only refer to the aluminium response curve and therefore can only be compared to the aluminium activation measurements (round

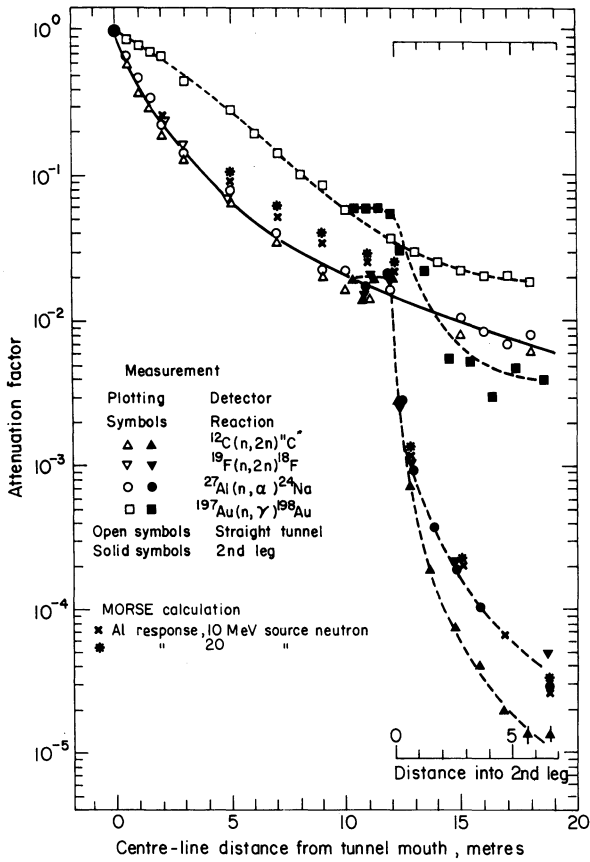


FIGURE 9 The calculated neutron attenuation in the first and the second leg compared with the measurements.

symbols). All results are normalized to unity at the mouth of the legs (distance zero). From Figs. 5 to 9 it can be seen that the calculation and the measurement agree with each other very well in the second leg if one takes into account the 20% standard deviation in the calculation. In the case of the 1.5 MeV neutron source (see Fig. 6), the calculated attenuation curves are systematically higher than the measured ones. This may result from the fact that the source energy (1.5 MeV) is too low, so that the responses at the mouth of the second leg were underestimated. The mouth of the second leg (detector number 3, see Fig. 3) has a direct view of the source. At this point the direct neutrons and the neutrons with energy just below the source energy dominate the radiation field. The moderated indium was also sensitive to some of these neutrons (above 1.5 MeV). Thus a calculation using a 1.5 MeV source would not take these neutrons into account and would underestimate the response at this point. On the

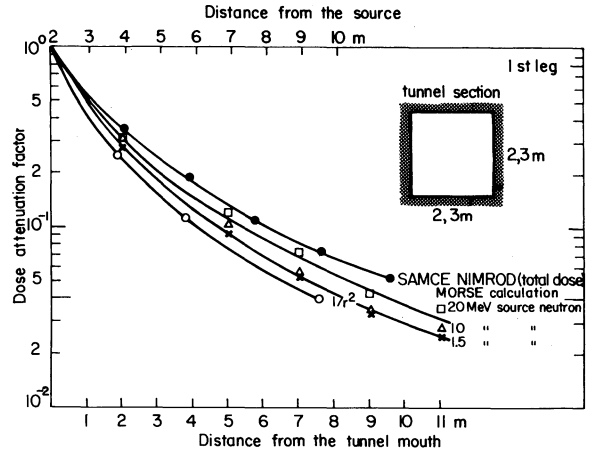


FIGURE 10 The calculated dose equivalent attenuation in the first leg compared with the inverse square law and the "SAM-CE" calculation.

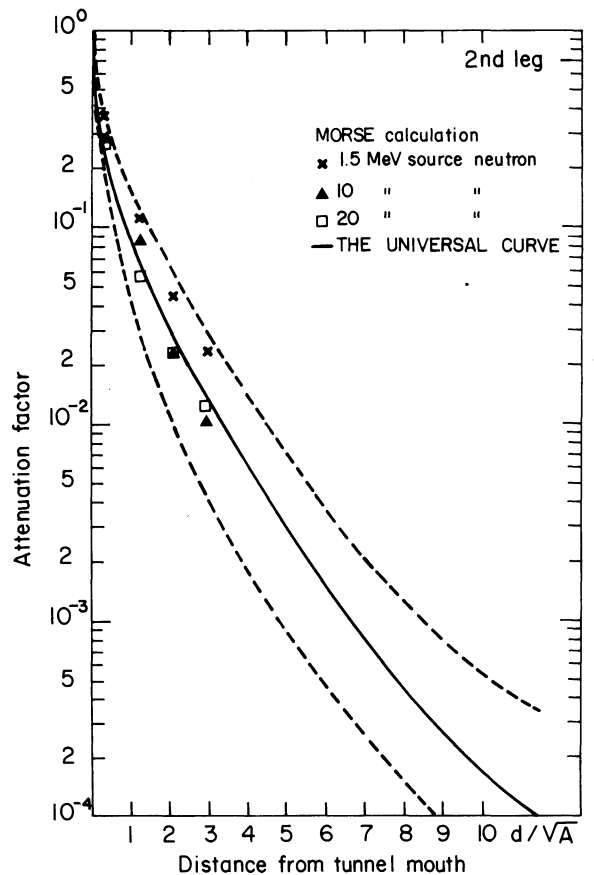


FIGURE 11 The calculated dose equivalent attenuation in the second leg compared with the universal curve.

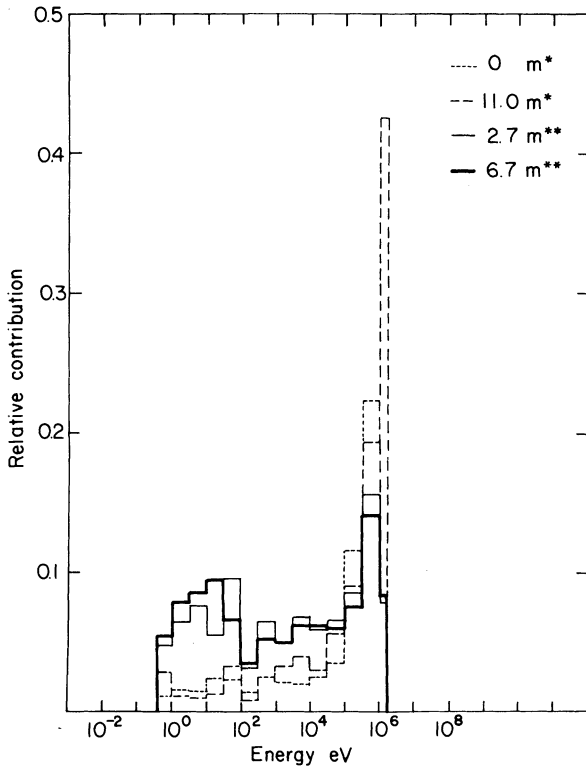


FIGURE 12 Relative flux distribution in the NIMROD tunnel for 1.5 MeV source neutrons. Dashed lines (*) are for distances from the mouth of the first leg, continuous lines (**) from the mouth of the second leg.

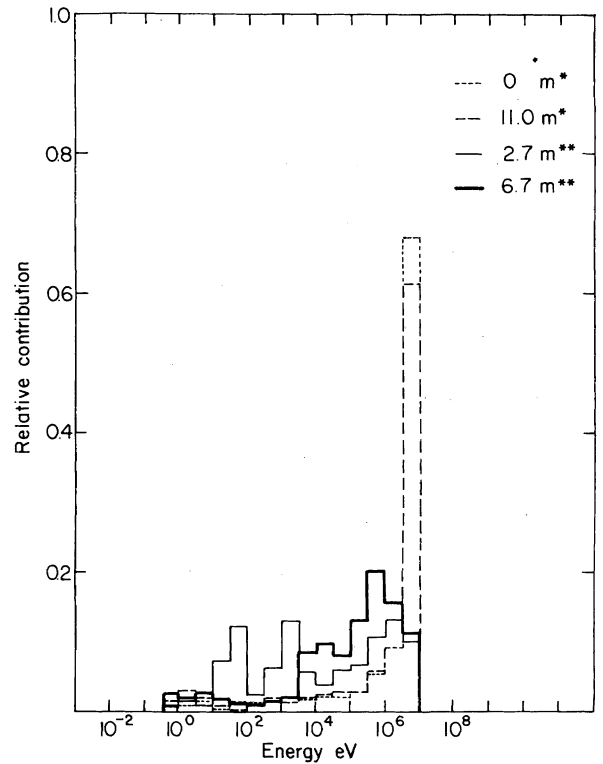


FIGURE 13 Same as Fig. 12 for 10 MeV source neutrons.

TABLE III
The Relative Dose Equivalent Contribution in the NIMROD Tunnel

Source energy (MeV)	Energy group (No.)	Lower energy edge (eV)	Percentage contribution of one neutron group (re-divided) to total dose equivalent (%)							
			1	2	3	4	5	6	7	
1.5 MeV		1.81×10^6								
	1	1.58×10^5	97.9	96.8	97.4	89.6	86.6	86.4	79.0	
	2	1.00×10^5	0.6	0.9	0.7	2.8	2.6	2.6	3.1	
	3	1.03×10^4	0.8	1.3	0.8	3.8	4.4	4.2	4.2	
	4	thermal	0.9	0.9	1.0	3.8	6.6	6.8	13.3	
10 MeV		1.00×10^7								
	1	3.16×10^6	84.0	82.7	83.6	40.4	31.1	31.2	27.2	
	2	2.00×10^6	5.3	5.1	3.7	17.2	17.6	17.8	14.2	
	3	1.58×10^5	9.8	11.0	11.5	37.5	43.7	45.2	52.2	
	4	1.00×10^5	0.2	0.3	0.3	0.7	1.5	1.2	2.4	
	5	1.03×10^4	0.3	0.5	0.3	2.8	2.3	1.9	2.7	
	6	thermal	0.1	0.5	0.6	1.5	3.8	2.8	1.3	
20 MeV		1.96×10^7								
	1	1.00×10^7	76.4	57.0	73.0	20.0	15.2	10.4	11.5	
	2	3.16×10^6	6.8	13.6	6.3	14.5	18.9	17.7	16.5	
	3	2.00×10^6	5.0	8.3	5.4	18.2	15.1	14.0	17.5	
	4	1.58×10^5	10.9	20.1	13.6	41.3	44.1	50.0	45.4	
	5	1.00×10^5	0.3	0.6	0.5	1.2	1.5	1.8	1.2	
	6	1.03×10^4	0.4	0.5	0.4	1.5	2.0	2.8	2.4	
	7	thermal	0.3	0.1	0.7	3.3	3.1	3.2	5.3	

other hand, the spectrum in the second leg is much "softer." The calculation would not underestimate the responses so much as in the first leg. In consequence, the curve shows a slower attenuation.

The agreement between calculation and measurement is not good in the first leg. The dose attenuation curve does not obey the inverse square law either (see Fig. 10), possibly because in the real situation the radiation field in the first leg was dominated by the high-energy particles and the neutrons fed by them via down-scattering in the first leg; MORSE is not able to simulate the high-energy process. The results obtained from this calculation also showed that the flux ratio of non-scattered neutrons to the total neutrons was about 0.3–0.35 in the first leg, and the dose equivalent ratio was 0.5–0.55. Therefore an inverse square law would not be applicable here. (Perhaps it would apply if the high-energy par-

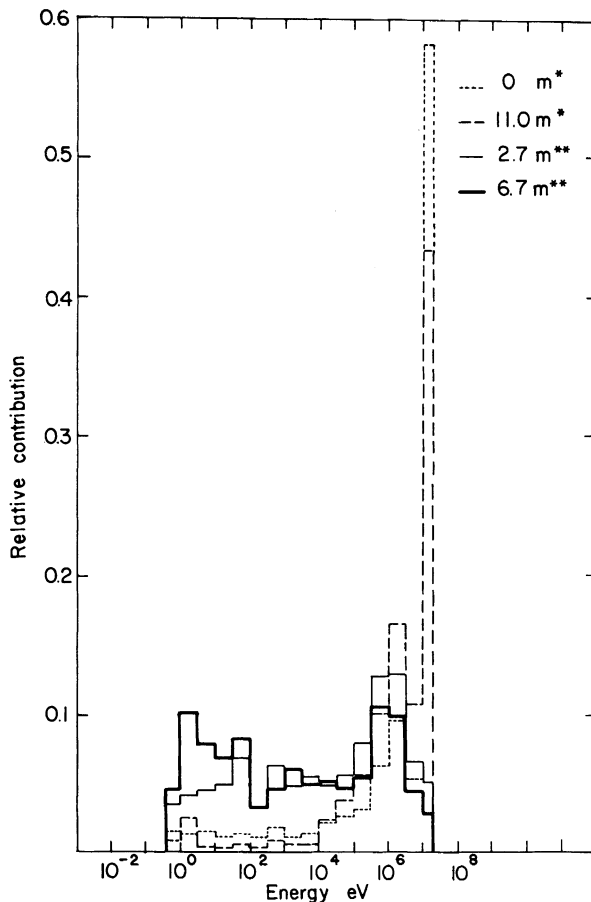


FIGURE 14 Same as Fig. 12 for 20 MeV source neutrons.

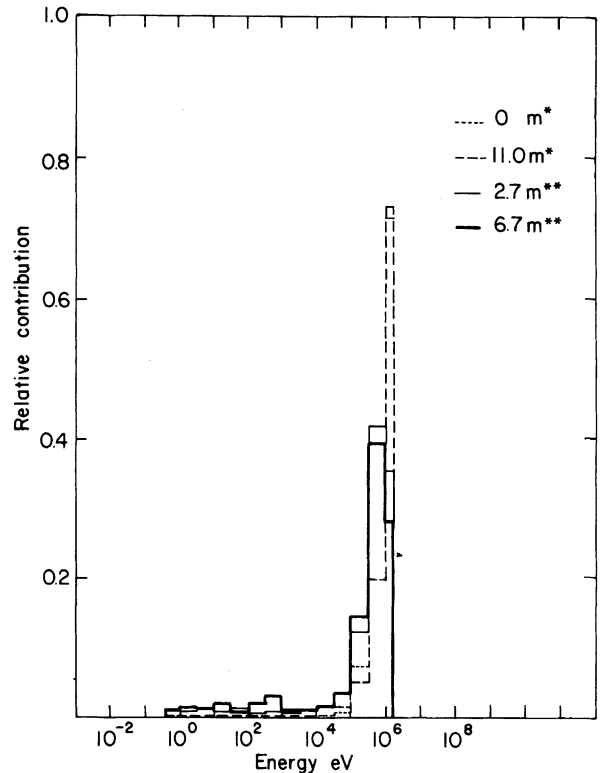


FIGURE 15 Relative dose equivalent distribution in the NIMROD tunnel for 1.5 MeV source neutrons. Dashed lines (*) are for distances from the mouth of the first leg, continuous lines(**) from the mouth of the second leg.

ticles were taken into account, as in the real situation.)

Goebel et al. plotted a set of generalized curves¹⁸ for duct calculations. A comparison with these curves is also illustrated in Fig. 11. The attenuation curves calculated for 10 MeV and 20 MeV source neutrons agree quite well with the "universal curve" in the second leg.

The contribution of neutrons in different energy groups is illustrated in Figs. 12 to 17: Figs. 12 to 14 are for flux and Figs. 15 to 17 for dose equivalent.

In the first leg the neutrons with energy ranging from the source energy to the energy just below the source energy are the absolutely prevailing components. The relative contribution of these neutrons to the total flux can be up to 65%, and 80% to the total dose equivalent. Here we must pay attention to the fact that the high-energy particles were not taken into account in this calculation. It can be imagined that the high-energy

particles dominate the radiation field in the first leg of a high-energy accelerator tunnel.

The situation is different in the second leg. In the energy range from 0.15 MeV to 3 MeV the peak contribution appears to be rather independent of the source energy (except 1.5 MeV source neutrons). More detailed data (in this energy region) are given in Table III. From this table it can be seen that over 60% of the dose equivalent comes from the neutrons with energy between 0.15 MeV and 3 MeV, in which approximately 50% of the total comes from the neutrons from 0.15 MeV to 2 MeV. This happens to be the energy range of the giant-resonance neutrons. Nevertheless, certain attention should be paid to the neutrons with energy just below the source energy, which contribute also about 20% to the total dose equivalent—a non-negligible portion. Furthermore, these neutrons are more penetrating.

From Figs. 15–17, a quasi-equilibrium of the dose equivalent spectrum can be seen from a depth of 2.5 m in the second leg. This is the reason why, for source energies above a few MeV, the dose equivalent attenuations derived

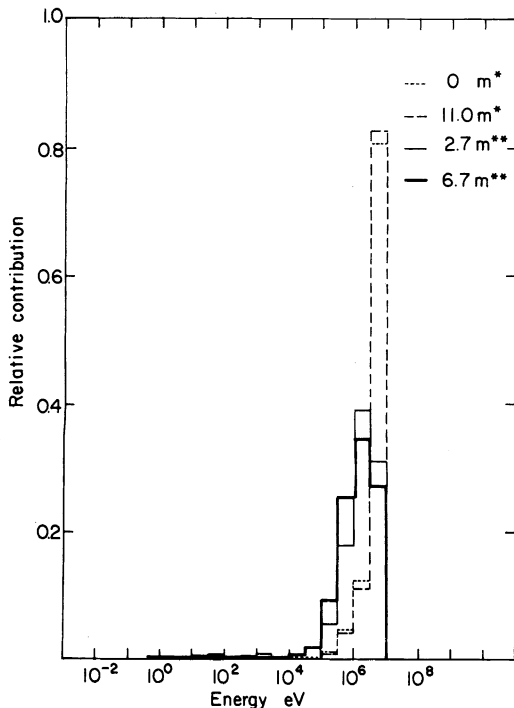


FIGURE 16 Same as Fig. 15 for 10 MeV source neutrons.

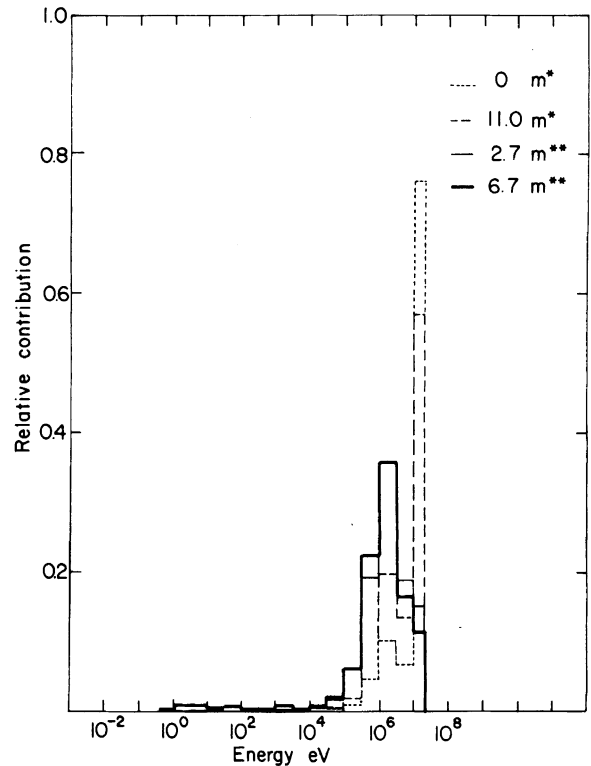


FIGURE 17 Same as Fig. 15 for 20 MeV source neutrons.

from MORSE calculations agree quite well with the attenuations calculated with ZEUS for monoenergetic neutrons (see Figs. 6–8).

The fractional deviations of the results are about 15% in the first leg and 20% in the second leg.

6. CONCLUSIONS

The MORSE code using a monoenergetic isotropic source can be used to provide a good simulation of the transport of neutrons in the second leg of a high-energy accelerator tunnel and duct, but the source neutron energy should not be chosen lower than 4 MeV. The calculated attenuation is somewhat independent of the source energy in the range from several MeV to 20 MeV (see Fig. 9). The calculation results match the measurement¹ well in the second leg. But for a long leg or multileg tunnel, the albedo technique has to be used (one that is more precise than that already in the code); otherwise, the execution time for the program is unacceptably long. Since

high-energy particles dominate the radiation field in the first leg, the MORSE code, which is mainly for the neutrons and gammas at "reactor energies," is not able to simulate the physical phenomena in the first leg (or at the place having a direct view of the source), but if some special cross-section data (see, for example, Alsmiller and Barish¹⁹) are used, the code can deal approximately with the neutrons up to 400 MeV.

A quasi-equilibrium of the neutron spectrum appears about from 2.5 m and onwards in the second leg and up to 45% of the total dose equivalent (taking into account the contribution from thermal neutrons) in the second leg comes from the neutrons with energy ranging from 0.15 MeV to 2 MeV.

For the duct calculation of a high-energy proton accelerator installation, the "universal curves" given by Goebel et al.¹⁸ can be used as a good first approximation.

ACKNOWLEDGEMENTS

The author gratefully acknowledges the help of G. R. Stevenson who edited the text of this paper. Thanks are also due to A. Fassò and K. Burn for useful discussions and suggestions.

REFERENCES

1. G. R. Stevenson and D. M. Squier, *Health Physics* 24, 87 (1973).
2. K. B. Shaw, Neutron studies in shields and tunnels of the 7 GeV proton synchrotron NIMROD, Proc. Int. Conf. on Radiation Measurements in Nuclear Power, Berkeley Nuclear Laboratories, 1966 (CEGB, The Physics Society and the Institute of Physics, Gloucestershire, 1967), p. 201.
3. W. Schimmerling and M. Awschalom, *IEEE Trans. Nucl. Sci.* NS-16, 604 (1969).
4. W. S. Gilbert et al., 1966 CERN-LRL-RHEL shielding experiment at the CERN Proton Synchrotron, UCRL-17941 (1968).
5. R. E. Maerker and V. R. Chain, AMC, a Monte Carlo code utilizing the albedo approach for calculating neutron and capture gamma ray distributions in rectangular concrete ducts, ORNL-3964 (1967).
6. M. O. Cohen et al., SAM-CE, a three-dimensional Monte Carlo code for the solution of the forward neutron and forward and adjoint gamma-ray transport equations, Rev. A, DNA 2830-A, July 1972; Rev. B, DNA 2830 F-B, August 1973.
7. F. Gervaise and M. d'Hombres, Variante du programme ZEUS appliqué à des problèmes de tunnels, CEA-N-933 (1968).
8. E. A. Straker et al., The MORSE code—a multigroup neutron and gamma-ray Monte Carlo transport code, ORNL-4585 (1970).
9. M. B. Emmett, The MORSE Monte Carlo radiation transport code system, ORNL-4972 (1975).
10. H. G. Vogt, Monte Carlo calculations of the neutron transmission through the access ways of the CERN Super Proton Synchrotron, CERN 75-14 (1975).
11. R. W. Roussin and J. B. Wright, Abstracts of the data library packages assembled by the Radiation Information Center, ORNL-RSIC-30 (Rev. 1973).
12. D. E. Bartine, J. R. Knight, J. V. Pace III, and R. W. Roussin, Production and testing of the DNA few-group coupled neutron-gamma cross-section library, ORNL/TM-4840 (1977).
13. T. Jenkins, private communication.
14. D. M. Hargreaves and G. R. Stevenson, Interpretation of results from the activation of indium, gold and cobalt disks in wax moderators, RHEL Internal Report RP/PN/37 (1969).
15. D. I. Garber and R. R. Kinsey, Neutron cross sections, BNL 325, Third Edition, Volume II (1976).
16. Data for protection against ionizing radiation from external sources, ICRP Publication 21 (1973).
17. P. J. Gollon and M. Awschalom, The design of penetrations in hadron shields, Proc. Int. Congress on Protection against Accelerator and Space Radiation, Geneva, 1971 (CERN 71-16, Geneva, 1971), p. 697.
18. K. Goebel, G. R. Stevenson, J. T. Routti, and H. G. Vogt, Evaluating dose rates due to neutron leakage through the access tunnels of the SPS, CERN LABII-RA/Note/75-10 (1975).
19. R. G. Alsmiller Jr. and J. Barish, Neutron-photon multigroup cross-sections for neutron energies < 400 MeV, ORNL/TM-7818 (1981).